# First measurements from the Laser Straightness Monitor of the LiCAS Rapid Tunnel Reference Surveyor *

Gregory Moss, Patrick Brockill, Sigal Cohen, John Dale, Yanmei Han, Tony Handford, Mark Jones, Lee Rainbow,Armin Reichold, Mike Tacon, Cecilia Uribe-Estrada, Stephanie Yang
John Adams Institute for Accelerator Physics, University of Oxford, UK
Johannes Prenting, Markus Schlösser, DESY, Hamburg, Germany
Grzegorz Grzelak, University of Warsaw, Warsaw, Poland

*Abstract*

The Laser Straightness Monitor (LSM) is a core part of the LiCAS Rapid Tunnel Reference Surveyor (RTRS). The system has been commissioned; first data has been taken and used to analyse mechanical stability of the RTRS. The first data and its implications will be shown. Two complementary calibration paradigms have been developed; one of which only very weakly relies on external witness measurements. Experiments are under way to confirm model predictions. These procedures will be explained and provisional results will be shown.

## THE RTRS

The RTRS is designed to accurately survey a network of reference points along the length of the International Linear Collider (ILC) tunnel. A full overview of the system is given in [1] and the current status is given in [2].

There are four subsystems of the RTRS: Internal FSI, external FSI, tilt sensors and the LSM. The LSM is used to measure the x & y translations of each unit, as well as the x and y rotations of each unit.

## LSM BASICS

The principle of the LSM is straightforward. A laser beam is directed down the length of the RTRS through an evacuated tube. It is reflected with a combination of a mirror and retro reflector to give an anti-collinear return beam. Each measurement unit has two pellicle beam splitters with a thickness of 2 microns at 45 degrees to the x axis of the unit. Each pellicle reflects approximately 10% of the light almost vertically onto a CCD camera which is used to determine the position of the spot. The returning light is reflected off the same pellicles onto cameras on the opposite side of the unit. Camera 0 is the first camera hit, followed by camera 2, the returning beam hits camera 3 and then camera 1. (See figure 1.)

Once the spot positions on all four cameras of the unit are known the x position, y position, the rotation around the x axis (Rot-x) and the rotation around the y axis (Rot-y) can be calculated. In principle, only two cameras are needed for this calculation but the RTRS units have four cameras for greater precision and accuracy.

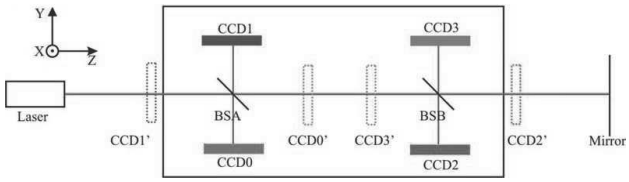


Figure 1: Schematic of the LSM system with one unit. The solid boxes indicate the CCDs in their actual positions. The dashed boxes show the equivalent linear positions.

## BEAM FITTING AND STABILITY

The position of the laser beams on the CCDs are found using two methods; fitting the projections of the image with one-dimensional Gaussians in both the x & y axes and a full two-dimensional multiple beam fitting procedure. For single beams with a clean Gaussian shape both methods have similar sub micron performance. The fitted beams in this paper have been produced using the projection fitting due to its large speed advantage.

A data taking run of 90 hours was performed with two sets of ten images being taken by each camera every 10 minutes. Due to a number of interruptions the data is not continuous and 50 hours into the run the intensity of the laser beam was increased by 50%. The effect of this can be seen in the plots in figure 3. The resolution histograms are for data taken after 50 hours. Figure 2 shows the x and y resolution of camera 0 on car 1. This launch is 200 mm from the image of this camera and is physically connected to the unit. The large difference in resolution between the x and y directions was not evident in the laboratory and is not currently understood. A possible cause is launch mount instability.

Plotting the fitted y position of the beam on camera 0 for each of the cars (see figure 3) clearly shows both noise and longer term motion of the beam. The camera image distances from the launch are 0.20m, 4.70m and 9.20m for

* Work supported by STFC in the LC-ABD collaboration and by the Commission of the European Communities under the 6th Framework Programme Structuring the European Research Area, contract number RIDS-011899.

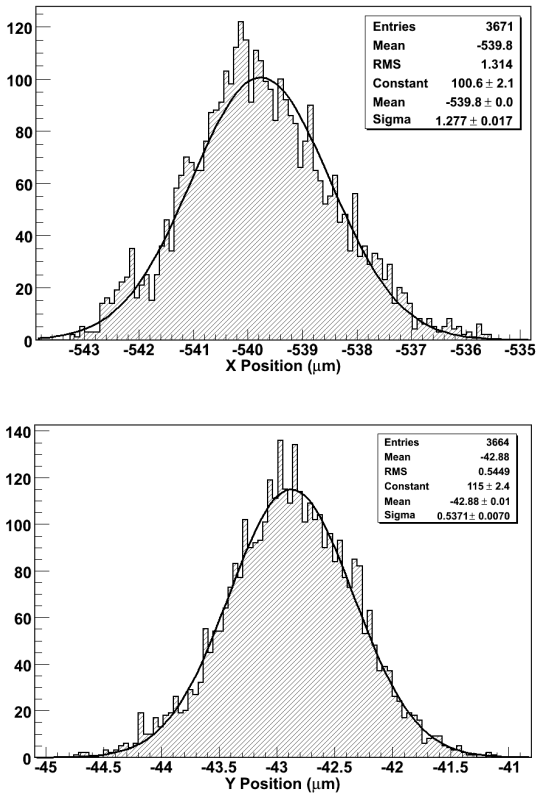


Figure 2: A histogram of the fitted x&y positions of the beam on car 1 camera 0 over a 40 hour period.

cars 1, 2 and 3 respectively. Camera 0 was chosen for each car as it is insensitive to the rotation of its car. (Note that the image of the camera in figure 1 is very close to the axis of rotation of the unit - the true lever arm is 1.2mm.) The plots show that the beam moves through an angle of 4 micro-radians over the 90 hours. Car 1 was touched at 50 hours which may explain some of the motion.

The same plot was also made for camera 2 on car 2 (at the bottom of figure 3). As the image of this camera is inverted the motion is the opposite to the motion on camera 0. There is a clear correlation confirming that the beam itself is moving rather than the motion being an artifact. The fitted positions for the two cameras are added and the data about 50 hours histogrammed to produce histogram 4. Its width of 0.78 microns is consistent with two independent Gaussian distributions with widths of 0.55 microns - the same value as found for the camera on the first car.

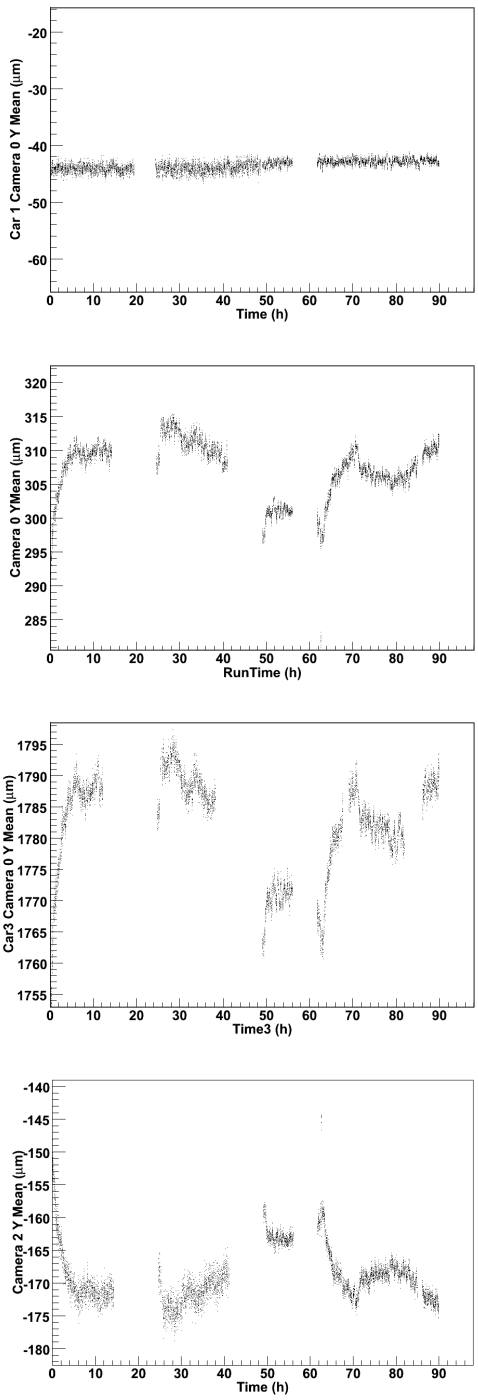


Figure 3: Fitted beam position on camera 0 on car 1 (top), car 2 (upper-middle) and car 3 (lower-middle). The bottom plot shows the corresponding data for camera 2 on car 2.

## RECONSTRUCTION

To predict the spot positions on each camera for a particular setup and orientation a ray-tracer was written. An optical setup can be entered into the ray-tracer and it will output the laser spot positions on all cameras, (a beam spot set,) including secondary and tertiary spots caused by multiple reflections. The ray-tracer can be used to find the orientation and position that result in a particular beam spot set. To do this a ray-trace is performed and the spots produced are compared to the input data. The orientation and position of the unit in the ray-tracer is then changed until the summed quadratic deviation of the ray-tracer spots from the measured spots is minimised. (See figure 5.)

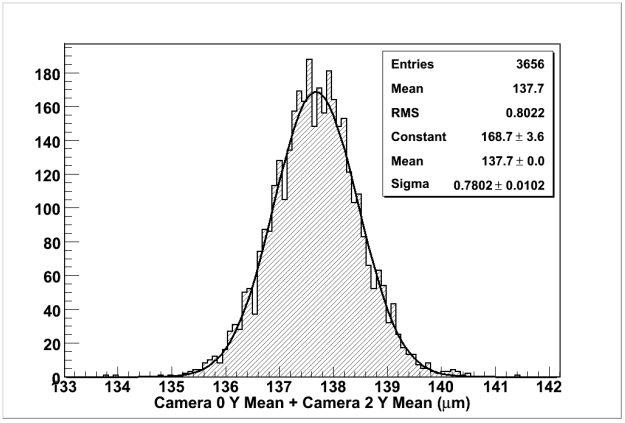


Figure 4: A histogram sum of the beam y position for cameras 0 and 2 on car 2 taken over a 40 hour period. The standard deviation of a fitted Gaussian (0.78 microns) is consistent with two uncorrelated cameras with a resolution of 0.55 microns. This matches the result shown in figure 2.

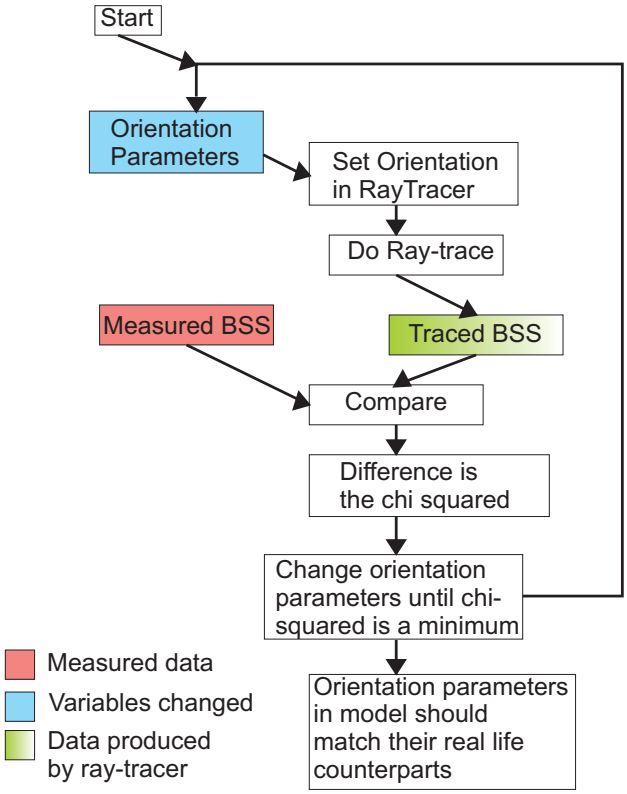


Figure 5: A flow chart describing the reconstruction procedure.

## GEOMETRY AND CALIBRATION CONSTANTS

To effectively reconstruct the LSM co-ordinates the positions of the internal components need to be known to a high level of accuracy. The positions and orientations of the elements of the LSM are the calibration constants. In order to derive the relative importance of the constants many ray-traces were performed, each with a different set of calibration constants. Each ray-trace produces a set of beam positions. From the beam spot set the LSM co-ordinates (x, y, Rot-x, Rot-y) can be reconstructed as described earlier. The reconstructed LSM co-ordinates are compared to the truth giving residuals. These residuals are then plotted against each of the calibration constants. The gradient of each plot gives the dependence of the reconstructed parameter residual on the calibration constant of interest. Note that this does not find any covariances but in the setup the errors are fairly independent. This is due to the small angles involved ($\pm$30 miliradians). Covariances can be observed by plotting the residual against two constants at the same time.

## CLASSICAL CALIBRATION

Two methods have been proposed to derive the calibration constants. The method described in this section relies on a witnessing system. In effect, it changes the constants until the two systems are consistent with each other.

The unit takes data in a number of different orientations while being observed with a laser tracker. The laser tracker data is then fed into the ray tracer which is used to give expected CCD spot positions. These spot positions are then compared with the measured spot positions. The process is then repeated with with modified calibration parameters until the differences between the expected and actual spot positions is minimised. At this point the calibration constants in the ray-tracer model match their real-life counterparts. (See figure 6)

A single calibration using the following typical values was performed:

- 1m camera resolution
- 3$\mu$m/10$\mu$radian observation error
- 80 orientations used
- 0.1mm component uncertainty

The constants found are shown in figure 2. The constants as defined in figure 1 do not quite match the constants in this simulation becuase for calibration an equivalent linear model was used. (See figure 1). This has the effect of absorbing the beam-splitter constants into the camera positions and exchanging the y and z axes. The important constants were found to less than 1 micron while other constants were found much less well. The CCD rotation angles were found so poorly that they were excluded from the calibration step.

To find the effectiveness of the calibration method it is not how well it finds the constants that is important; it is how close the miscalibrated (i.e. using the constants found by the calibration method rather than their truth values) system can match real life. To this end the following procedure is followed:

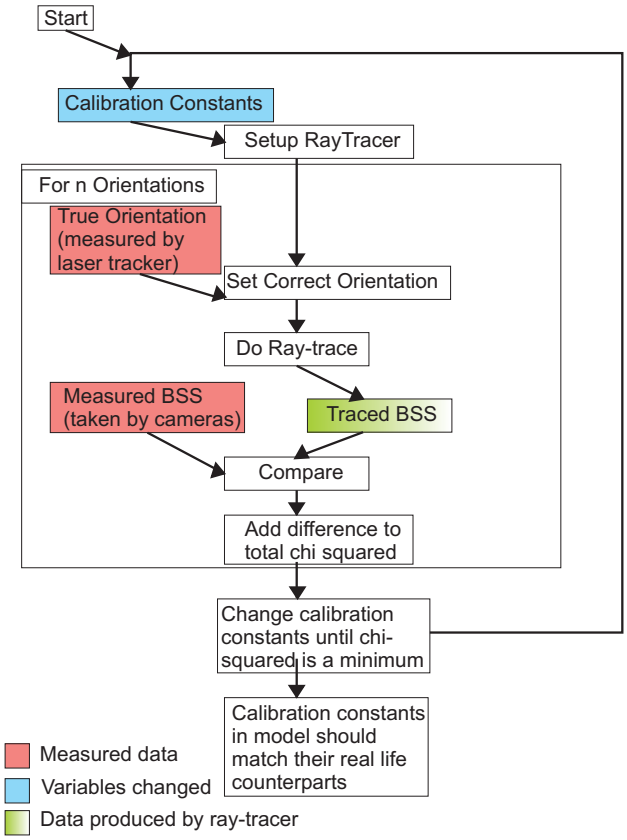


Figure 6: A flow chart of the classical calibration procedure.

- A ray-tracer model containing the true calibration constants is set to a particular orientation and position.
- A ray-trace is performed and a beam spot set it produced.
- A reconstruction is done using another model that has the calibration constants found by the simulated calibration run.
- The LSM co-ordinates produced by the reconstruction are compared with the truth.

This is repeated for many different orientations and positions producing the four histograms of the co-ordinate residuals. (See figure 7.) The mean of each histogram gives the systematic offset caused by the miscalibration. The width of each histogram gives the precision of the reconstruction. These widths are primarily due to the accuracy of the spot position measurements - if these errors are turned off then the widths are much narrower. These resolution effects dominate the width caused by co-variances between the errors and the positions & orientations.

The results in figure 7 are only an example for one set of constants. We need to know what to statistically expect for a typical car. To this end the whole procedure is repeated many times. Each time the systematic offset for each reconstruction variable is added to a histogram, with

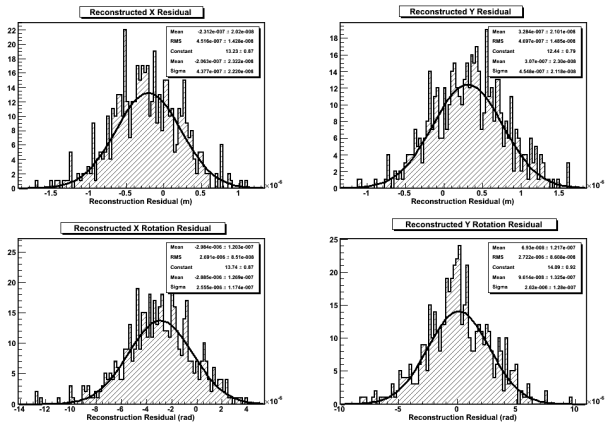


Figure 7: A single calibration simulation. The histograms show the x, y, rot-x & rot-y residuals of many reconstructions over a range of $\pm 2$ mm and $\pm 2$ milliradians for a typical unit after a calibration run. The offsets are -0.21$\mu$m, 0.31$\mu$m, -2.89$\mu$radians and 0.10$\mu$radians respectively. The standard deviations are 0.43$\mu$m, 0.45$\mu$m, 2.56$\mu$radians and 2.62$\mu$radians.

the standard deviation added to another. At the end of the process there are eight histograms; Offsets for y, y, rot-x & rot-y as well as the standard deviations, two example are shown in figure refCalibrationrunXhists. The histograms of the offsets have two properties. Firstly, the mean is near zero indicating that there is little bias to a particular direction. Secondly, the standard deviation of the offset histograms give the expected precision of a system which has been calibrated in the above way. For example, the RMS of the x error is 0.33 microns. This means (assuming a normal distribution) that a car calibrated using the method and parameters described will give a magnitude of systematic offset in reconstructed x position of $<$ 0.33 microns 68% of the time. The histograms of the standard deviations are also useful. The mean value gives the expected precision of the unit. The spread of the standard deviation is small as would be expected as the cameras have an unchanging resolution. With a larger number of reconstructions in the simulation this spread is expected to reduce. The results of this simulation can be found in table 3. They are better than the target of 1 micron for translations and near the target of 1 micro-radian for rotations.

## AUTO-CALIBRATION

The second method of calibration is to include the constants as part of the fit. This has the advantage that a much larger amount of data can be used and no witnessing system is needed. The procedure is shown in figure 9. In effect, it adjusts the calibration constants to minimise the sum of $\chi^2$s from the reconstructions. In theory, all data ever taken can be included in this fit though in practice some data would be retained as a check. In addition, by selecting data over different epochs any change of constants over time can be

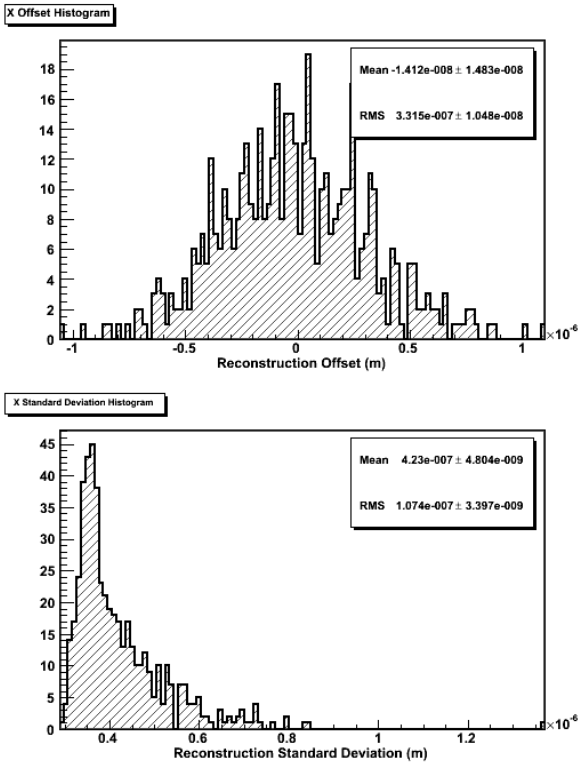


Figure 8: The Calibration simulation results for the LSM x co-ordinate. It is representative of the other histograms produced.

| Histogram | Mean (m) | SD (m) |
|---|---|---|
| X Offset | $-1.4\times10^{-8}$ | $\mathbf{0.33}\times10^{-6}$ |
| Y Offset | $8.6\times10^{-9}$ | $\mathbf{0.34}\times10^{-6}$ |
| X SD | $\underline{0.42\times10^{-6}}$ | $1.1\times10^{-7}$ |
| Y SD | $\underline{0.42\times10^{-6}}$ | $1.1\times10^{-7}$ |
| **Histogram** | **Mean (rad)** | **SD (rad)** |
| Rot-x Offset | $1.6\times10^{-8}$ | $\mathbf{1.1}\times10^{-6}$ |
| Rot-y Offset | $-3.2\times10^{-8}$ | $\mathbf{1.2}\times10^{-6}$ |
| Rot-x SD | $\underline{2.4\times10^{-6}}$ | $2.6\times10^{-7}$ |
| Rot-y SD | $\underline{2.4\times10^{-6}}$ | $2.6\times10^{-7}$ |

Table 3: Summaries of the calibration simulation histograms. The bold values give the accuracy for that LSM co-ordinate while the underlined text gives the precision.

seen. This procedure does have some challenges - it is blind to collective changes; for example, if all cameras are moved x microns laterally then the total $\chi^2$ would remain the same even though the reconstructed values would have an offset of -x microns. However, the fit still converges and these ambiguities can be removed if the process is combined with the classical method described earlier. In addition, it is expected that most, if not all of them will be fixed when the various systems are combined due to the overlap in measured parameters. If the collective changes are corrected for manually the auto-calibration produces very similar results to the classical procedure. It generally gives sub micron performance for the important constants with worse performance for others. The exact values vary but depend on the run parameters.

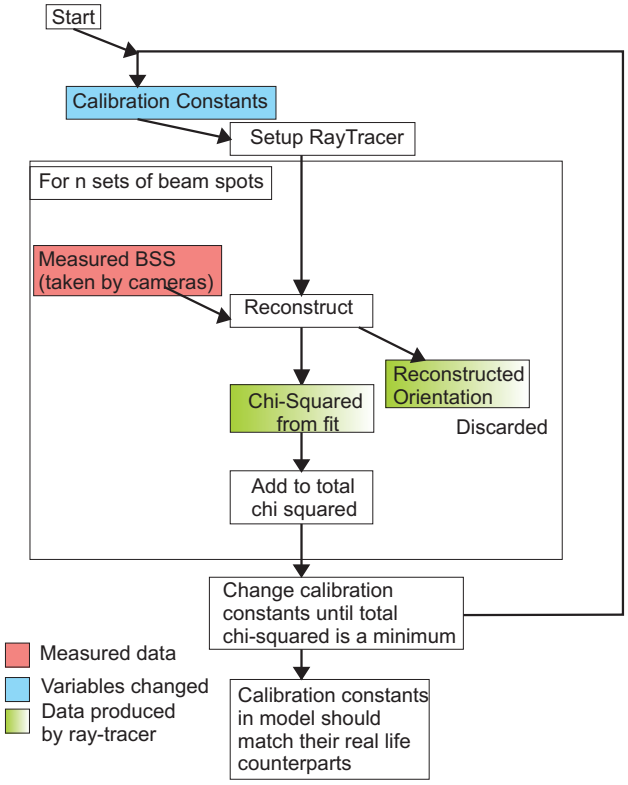


Figure 9: A flow chart of the auto-calibration procedure

## CONCLUSIONS

We now posses a working LSM system. The beam fitting is now reliable and accurate enough for reconstruction. The stability of the system is currently under investigation. The ray-tracer is well developed and is effective at co-ordinate reconstruction. Calibration simulations are encouraging with both simulations producing predictions that are accurate enough. They should compliment the SIMULGEO and linear algebra methods also being developed[2].

## REFERENCES

[1] The LiCAS-RTRS A Rapid and Cost Efficient Survey System for the ILC A. Reichold for the LiCAS collaboration, Proceeding of the 9th International Workshop on Accelerator Alignment, SLAC, USA, September 2006, http://www.slac.stanford.edu/econf/C06092511/papers/WE008.PDF

[2] THE LICAS RAPID TUNNEL REFERENCE SURVEYOR – THE STATUS AFTER COMMISSIONING Armin Reichold for the LiCAS collaboration Proceedings of the the 10th International Workshop on Accelerator Alignment February 11-15, 2008 KEK, Tsukuba, Japan

| Constant | X ($\times 10^{-3}$) | Y ($\times 10^{-3}$) | Rot-x ($\times 10^{-3}$) | Rot-y ($\times 10^{-3}$) |
|---|---|---|---|---|
| True x | -0.0 | 0.2 | 1.5 | -0.3 |
| True y | -0.0 | 0.1 | 1.7 | -0.4 |
| True Rot-x_s | -0.1 | -0.0 | 0.5 | -0.4 |
| True Rot-y_s | -0.0 | 0.1 | 0.9 | -0.0 |
| BS0 x | 13.8 | -39.4 | -142.7 | -70.0 |
| BS0 y | 24.2 | 542.9 | 2407.3 | 33.1 |
| BS0 z | 9.2 | 510.6 | 2529.6 | 22.6 |
| BS0 Rot-x | 6.7 | -18.6 | 524.7 | 80.8 |
| BS0 Rot-y | -13.8 | 35.5 | -34.4 | 184.1 |
| BS0 Rot-z | 2.4 | 32.2 | 57.6 | -249.6 |
| BS1 x | -6.4 | 17.4 | -173.8 | -120.4 |
| BS1 y | 3.3 | 519.0 | -2448.6 | 44.1 |
| BS1 z | 9.0 | 519.7 | -2433.3 | 32.1 |
| BS1 Rot-x | -17.9 | 29.8 | 394.0 | 66.4 |
| BS1 Rot-y | -4.7 | 2.2 | 32.7 | 255.7 |
| BS1 Rot-z | -4.3 | -16.5 | -91.1 | -233.5 |
| CCD0 x | 247.6 | -11.2 | 69.1 | 15.2 |
| CCD0 y | -1.6 | -22.7 | -98.2 | 23.4 |
| CCD0 z | -2.9 | -237.1 | -55.0 | -56.6 |
| CCD0 Rot-x | -6.8 | -18.7 | -366.8 | 14.5 |
| CCD0 Rot-y | 0.8 | 9.2 | -80.2 | -21.1 |
| CCD0 Rot-z | 9.4 | 8.5 | 98.4 | -48.2 |
| CCD1 x | 255.2 | 6.3 | 102.5 | -2430.7 |
| CCD1 y | -0.6 | 7.0 | -78.1 | 6.1 |
| CCD1 z | 2.6 | -233.6 | -2635.2 | 15.4 |
| CCD1 Rot-x | 3.8 | -12.5 | 162.8 | 75.9 |
| CCD1 Rot-y | 3.8 | 28.3 | 21.2 | -27.1 |
| CCD1 Rot-z | -0.0 | 34.9 | -4.7 | -162.7 |
| CCD2 x | 249.9 | 31.6 | 101.8 | 2427.0 |
| CCD2 y | 1.4 | -32.8 | 34.7 | -103.6 |
| CCD2 z | 1.8 | -237.2 | 2472.3 | 7.1 |
| CCD2 Rot-x | 20.7 | -0.9 | 265.9 | -10.2 |
| CCD2 Rot-y | -9.9 | -29.0 | 174.6 | -35.4 |
| CCD2 Rot-z | 1.2 | 7.5 | -150.5 | -55.1 |
| CCD3 x | 248.8 | 61.1 | -88.8 | -83.4 |
| CCD3 y | -1.2 | -8.1 | -101.6 | 76.3 |
| CCD3 z | 4.2 | -245.9 | 187.3 | 23.4 |
| CCD3 Rot-x | 3.9 | 28.0 | 17.7 | 40.7 |
| CCD3 Rot-y | 3.0 | -15.2 | -9.8 | -74.5 |
| CCD3 Rot-z | -16.5 | 28.4 | -43.3 | -57.6 |

Table 1: Calibration constant fractional importance for each LSM co-ordinate. A value of $1\times10^{-3}$ means for a 1 mm(miliradian) error in the constant, that reconstructed co-ordinate will have an error of 1 micron ($\mu$radian).

| Parameter | FittedValue | TrueValue | Error |
|---|---|---|---|
| CCD0X: | $1.841\times10^{-6}$ | $1.660\times10^{-6}$ | $1.81\times10^{-7}$ |
| CCD0Y: | $8.7949\times10^{-5}$ | $8.8319\times10^{-5}$ | $-3.69\times10^{-7}$ |
| CCD0Z: | -0.001472973 | -0.001163118 | $-3098.56\times10^{-7}$ |
| CCD1X: | $-3.3726\times10^{-5}$ | $-3.4036\times10^{-5}$ | $3.10\times10^{-7}$ |
| CCD1Y: | $2.5746\times10^{-5}$ | $2.5474\times10^{-5}$ | $2.72\times10^{-7}$ |
| CCD1Z: | -0.200587994 | -0.200248126 | $-3398.68\times10^{-7}$ |
| CCD2X: | $8.6166\times10^{-5}$ | $8.5915\times10^{-5}$ | $2.51\times10^{-7}$ |
| CCD2Y: | $-4.5010\times10^{-5}$ | $-4.4121\times10^{-5}$ | $-8.89\times10^{-7}$ |
| CCD2Z: | 0.200060178 | 0.200130245 | $-700.67\times10^{-7}$ |
| CCD3X: | 0.000100020 | $9.9858\times10^{-5}$ | $1.62\times10^{-7}$ |
| CCD3Y: | $3.8873\times10^{-5}$ | $3.9206\times10^{-5}$ | $-3.32\times10^{-7}$ |
| CCD3Z: | 0.000987289 | 0.001231625 | $-2443.36\times10^{-7}$ |

Table 2: Calibration constants found using classical calibration with 80 loops, 1 micron beam blurring and 3 micron / 10 microradian tracker errors.